RevMexAA (Serie de Conferencias), **36**, 149–154 (2009)

MAGNETIZED DISKS AROUND YOUNG STARS

S. Lizano,[1] F. H. Shu,[2] D. Galli,[3] and A. Glassgold[4]

RESUMEN

Discutimos la estructura y evolución de discos magnetizados en torno a estrellas jóvenes que han arrastrado su campo magnético en el proceso de colapso gravitacional. El disco evoluciona debido a dos procesos difusivos: estreses viscosos que redistribuyen la masa y el momento angular, y la difusión resistiva de masa a través de líneas de campo magnético debido a la conducción imperfecta. En estado estacionario existe un modelo analítico de la estructura de estos discos magnetizados. Discutimos la aplicación de este modelo a discos alrededor de estrellas jóvenes de alta y baja masa y resultados recientes de modelos dependientes del tiempo.

ABSTRACT

We discuss the structure and evolution of a magnetized accretion disks around young stars that have dragged their magnetic field in the process of gravitational collapse. The disk evolves due to two diffusive processes: viscous stresses that redistribute mass and angular momentum, and the resistive diffusion of mass across magnetic field lines due to imperfect conduction. In steady-state there is an analytic model of the structure of these magnetized disks. We discuss the application of this model to disks around low and high mass young stars and recent results of time dependent models.

Key Words: accretion, accretion disks — ISM: magnetic fields — stars: formation — stars: pre-main sequence

1. GENERAL

Stars are formed in molecular clouds which have magnetic fields strong enough to affect their dynamics and evolution. During the phase of gravitational collapse, the magnetic field is dragged by the accretion flow. The dragged field can become so strong that it can produce a catastrophic magnetic braking of the infalling gas. Thus, the loss of some magnetic flux by dissipative effects in the inner regions of the cloud core is a necessary condition for the formation of protoplanetary disks (see review of Galli et al. 2009). Then, a disk of gas and dust is formed around the central star because the infalling gas has angular momentum and reaches a centrifugal barrier. As a result of the gravitational collapse of the central parts of such a magnetized core, one expects a poloidal field to be dragged into the accretion disk. The hourglass shape of the magnetic field lines predicted by the collapse of magnetized clouds has been recently observed by dust polarized emission with the SMA by Girart et al. (2006). Polarization vectors in the upper panel of Figure 1 are expected to be perpendicular to the magnetic field direction shown in the lower panel. Gonçalves, Galli, & Girart (2008) have recently modeled these observations.

Due to ohmic dissipation and ambipolar diffusion, some magnetic flux is lost from the inner regions of a cloud core such that the expected dimensionless disk mass-to-flux ratio is (Galli et al. 2006)

$$\lambda_0 = \frac{2\pi G^{1/2}(M_* + M_d)}{(\Phi_* + \Phi_d)} \sim 4\,, \qquad (1)$$

where M_* and Φ_* are the mass and magnetic flux of the star, and M_d and Φ_d are the mass and magnetic flux of the disk. As a result of viscous and resistive evolution, the mass of the disk becomes much smaller than the mass of the central star, $M_d \ll M_*$, and the angular momentum and the magnetic flux end up in the disk. Thus, accretion disks must be strongly magnetized.

Here we review the evolution of such magnetized accretion disks that evolve by viscous torques that cause the redistribution of mass and angular momentum, and by resistive diffusion of mass across the poloidal field that threads the disk (Shu et al. 2007a, hereafter S07). We consider the situation after the main accretion phase over the 4π steradians has passed, giving the geometry depicted by Figure 2 where mass accretion onto the star occurs mainly through the disk.

[1]Centro de Radioastronomía y Astrofísica, Universidad Nacional Autónoma de México, Apdo. Postal 3-72, 58090, Morelia, Michoacán, Mexico (s.lizano@crya.unam.mx).

[2]Department of Physics, University of California, San Diego, CA 92093, USA (fshu@physics.ucsd.edu).

[3]Osservatorio Astrofisico di Arcetri, Large E. Fermi 5, 50125 Firenze, Italy (galli@arcetri.astro.it).

[4]University of California at Berkeley, Astronomy Department, Berkeley, CA 94270, USA (glassgold@berekely.edu).

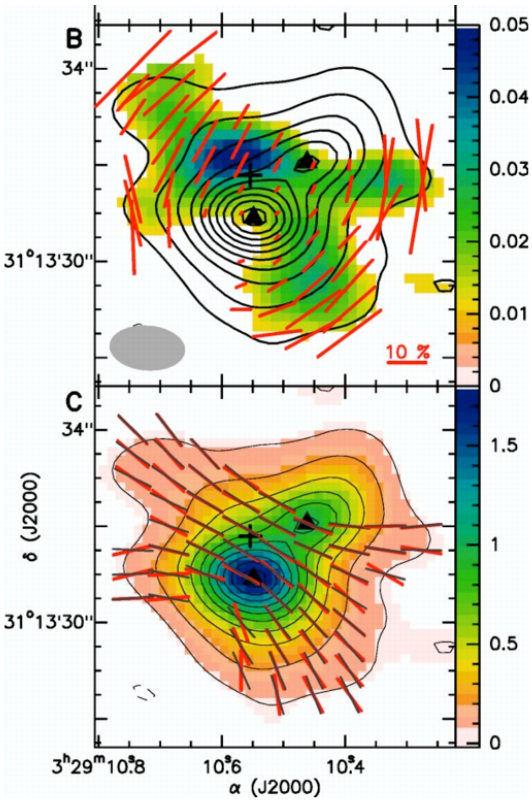

Fig. 1. Hourglass shape of the magnetic field toward NGC 1333 IRAS 4A (Girart et al. 2006).

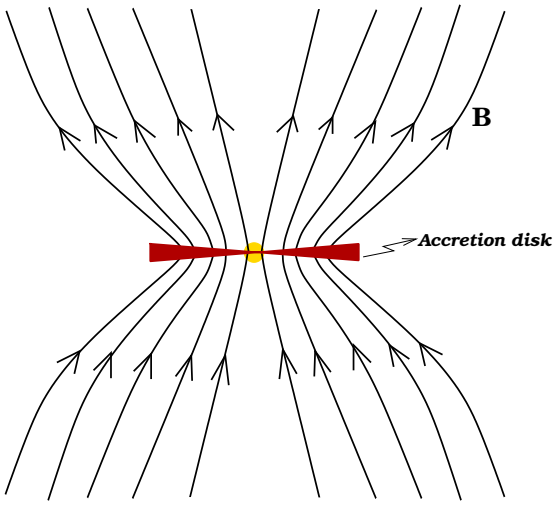

Fig. 2. Magnetic field lines threading an accretion disk.

The evolution of the disk is due to two diffusive processes in the system: "viscous torques" exerted by turbulent and magnetic stresses; and "resistive" redistribution of mass with respect to the magnetic flux due to imperfect conduction (ohmic dissipation, ambipolar diffusion, Hall effect).

This work extends the results of Lubow, Papaloizou, & Pringle (1994) who considered in, a kinematic approximation, the evolution of the magnetic field dragged in by viscous accretion and moving outward due to magnetic diffusivity. In steady-state, the dragging of field lines by accretion is balanced by the outward motion of the field due to magnetic diffusion. By including the force equation, our models show that the magnetic tension force makes the disk rotation sub-keplerian (S07). These models give the structure of disk around different type of young stars. At the end, we briefly discuss recent results on time dependent models.

2. STEADY-STATE THIN AXISYMMETRIC ACCRETION DISKS

We solve the integrated MHD equations of a thin accretion disk in steady-state. The equation of continuity is

$$\varpi \Sigma u = -\frac{\dot{M}_d}{2\pi}\,, \tag{2}$$

where Σ is the mass surface density, u is the radial speed, and $\dot{M}_d$ is the mass accretion rate through the disk. The equation of radial force balance is

$$\varpi \Omega^2 = -\frac{B_z B_\varpi^+}{2\pi\Sigma} + \frac{GM_*}{\varpi^2}\,, \tag{3}$$

where Ω is the angular speed, B_z is the vertical magnetic field, and B_ϖ^+ is the radial magnetic field just above the disk. In this equation, the disk self-gravity and the thermal and magnetic pressures have been ignored. In the RHS, the acceleration due to magnetic tension is the radial component of the Lorentz force, where the radial magnetic field is given by

$$B_\varpi^+ = \int_0^\infty K_0\left(\frac{r}{\varpi}\right) B_z(r,t)\,\frac{rdr}{\varpi^2}\,, \tag{4}$$

that takes into account the vacuum magnetic field outside the disk; K_0 is the gravity kernel of a thin disk (e.g., Shu et al. 2004). The torque equation that includes viscous stresses is

$$\dot{M}_d \varpi^2 \Omega = -2\pi\varpi^2 \Sigma \nu \varpi \frac{d\Omega}{d\varpi}\,, \tag{5}$$

where ν is the viscosity coefficient. An finally, the induction equation for B_z with a finite resistivity η is

$$B_z u = -\frac{\eta B_\varpi^+}{z_0}\,, \tag{6}$$

where z_0 is the disk half-thickness.

The continuity and the torque equations imply a radial speed

$$u = -\frac{\dot{M}_d}{2\pi\varpi\Sigma} = -\frac{\nu}{\varpi}\left(\frac{\varpi}{\Omega}\frac{d\Omega}{d\varpi}\right) .$$

Consistency of this accretion speed and that given by the induction equation imply that the angle of the magnetic field with respect to the disk and the ratio of the viscosity coefficient and the resistivity are related as

$$\frac{B^+_\varpi}{B_z} = \alpha^2(\varpi) \equiv -\frac{\nu}{\eta}\frac{z_0}{\varpi}\left(\frac{\varpi}{\Omega}\frac{d\Omega}{d\varpi}\right) . \qquad (7)$$

These equations allow an analytic solution where the partial support provided by magnetic tension against gravity causes a sub-keplerian rotation,

$$\Omega = f\left(\frac{GM_*}{\varpi^3}\right)^{1/2} , \qquad (8)$$

where the departure from keplerian rotation is $f < 1$. For a surface density that varies as a power law,

$$\Sigma = C\varpi^{-2\ell} , \qquad (9)$$

the function α^2 is a positive dimensionless constant,

$$\alpha^2 \equiv I_\ell = \int_0^\infty K_0(\xi)\xi^{-\ell}d\xi . \qquad (10)$$

The fact that α is constant implies that, for a given exponent ℓ, the ratio of the viscosity coefficient to the resistivity is proportional to the disk aspect ratio, z_0/ϖ, and that the inclination of the magnetic field at the disk surface is constant,

$$\frac{\eta}{\nu} = \frac{3}{2I_\ell}\left(\frac{z_0}{\varpi}\right) \ll 1; \qquad \text{and} \quad B^+_\varpi = I_\ell B_z . \qquad (11)$$

To obtain the disk structure one needs to specify the viscous or resistive mechanisms. Below we discuss the viscous stress.

2.1. *Magnetorotational Instability*

The viscous stress produced by the magnetorotational instability (MRI) is a very promising mechanisms to produce the required anomalous viscosity in accretion disks that will allow them to evolve in the observed short timescales, of only millions of years. This instability is due to the torque produced by the stretching of **B** by differential rotation. For an element of fluid displaced outward, the field will try to maintain rigid rotation, thus, the excess of angular momentum will increase the displacement even further provoking the instability for large

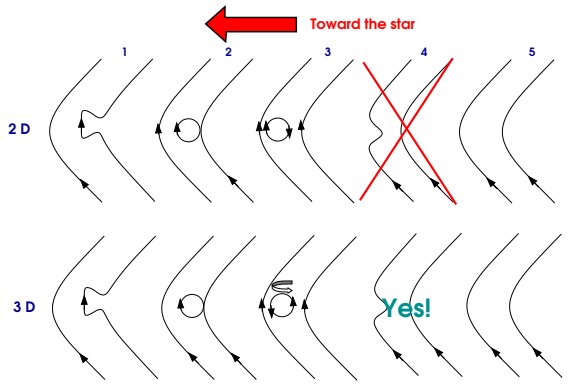

Fig. 3. Loop dynamics (S07).

enough wavelengths (Balbus & Hawley 1991). Lacking MRI simulations that are both global and with nonzero net magnetic flux, relevant for the young disks depicted in Figure 2, S07 considered mixing length arguments to estimate the viscous stress due to MRI. The toroidal field produced by the radial field stretched by differential rotation is given by

$$\delta B_\varphi \delta u \sim \delta B_\varpi \varpi \frac{d\Omega}{d\varpi}\delta\varpi , \qquad (12)$$

where $\delta\varpi$ is the radial mixing length and has the same sign as the velocity perturbation $\delta u \sim \Omega\delta\varpi$, and $\delta B_\varpi \sim B^+_\varpi$. The component of the Maxwell stress that exerts the torque integrated over the disk thickness, $\Pi_{\varpi\varphi}$ is then given by

$$\int_\infty^\infty \frac{\delta B_\varpi \delta B_\varphi}{4\pi}dz \sim \frac{(B^+_\varpi)^2}{2\pi}\frac{\varpi}{\Omega}\frac{\partial\Omega}{\partial\varpi}z_0 . \qquad (13)$$

The comparison of this result with the RHS of equation (5)

$$\Sigma\nu\varpi\frac{\partial\Omega}{\partial\varpi} ,$$

gives the viscosity coefficient for the MRI process as

$$\nu = D\frac{B_z^2 z_0}{2\pi\Sigma\Omega} , \qquad (14)$$

where we substituted the relation $B^+_\varpi = I_l B_z$, derived in steady-state. If good coupling exists (i.e., enough ionization), even though our models have dynamically important magnetic fields, the MRI condition that the magnetic pressure is less than the gas pressure, $v_A^2/a^2 < 1$, is always satisfied. This functional form of the viscosity, equation (14) and its relation to the resistivity equation (11), can be understood in terms of magnetic loops that carry mass and reconnect downstream to produce an appreciable mass transfer across field lines, greater that the

collisional values. This loop dynamics, shown in Figure 3, involves the bending and pinching of field lines by turbulent fluid motions. In the top cartoon, the magnetized loop tries to move downstream but in a 2D geometry reconnection is not possible because the magnetic field directions are parallel. On the other hand, if the loop is twisted out of the meridional plane it can reconnect downstream because its magnetic field direction is anti-parallel to the reconnection point, as shown in the bottom cartoon. The extra degree of freedom in 3D allows the twisting which changes the magnetic field direction in the loop. The functional relation between the viscosity and the resistivity, $\eta \propto (z_0/\varpi)\,\nu$, is explained because only a fraction of the loops will have the appropriate twisting.

3. ANALYTIC DISK MODEL

With MRI viscosity coefficient discussed above, one obtains the structure of a magnetized accretion disk in steady-state with sub-keplerian rotation, given by equation (8), a power-law vertical magnetic field

$$B_z = \left(\frac{2f}{3DA(\varpi)}\right)^{1/2} \left(\frac{GM_*\dot{M}_d^2}{\varpi^3}\right)^{1/4}, \qquad (15)$$

and a power-law surface density

$$\Sigma = \frac{f}{1-f^2}\left(\frac{I_\ell}{3\pi DA(\varpi)}\right)\frac{\dot{M}_d}{(GM_*\varpi)^{1/2}}, \qquad (16)$$

where the resistivity and the viscosity are given by

$$\eta = \frac{3A(\varpi)}{2I_\ell}\nu, \quad \text{and} \quad \nu = D\frac{B_z^2 z_0}{2\pi\Sigma\Omega}, \qquad (17)$$

and the disk aspect ratio is a power-law, $A(\varpi) \equiv z_0/\varpi \propto \varpi^{\frac{(4\ell-1)}{2}}$. The radial magnetic field, B_ϖ^+, is obtained from equation (11).

In fact, the disk aspect ratio depends on the local temperature, due to the heating and cooling processes, and the vertical force balance. While the thermal aspect ratio is given by $A_0 = (2a^2\varpi/GM_*)^{1/2}$, one expects that $A \leq A_0$, due to the magnetic compression of the pinched poloidal field.

To determine the value of f, one can compute a viscous-accretion radius, R_ν, such that the age of the system is given by the time to drain the disk, $M_d(R_\nu)/\dot{M}_d = t_{\rm age}$. This radius can be equated to the radius, R_Φ, that contains all the flux brought in by star formation, λ_0. Then, the deviation from keplerian rotation is given by

$$1 - f^2 = \frac{1}{2}\frac{(1-l)I_\ell}{\lambda_0^2}\frac{M_*}{M_d(R_\Phi)}. \qquad (18)$$

For a closed system in which infall has ceased, disk accretion must decrease the ratio of the disk mass to stellar mass, $M_d(R_\Phi)/M_*$. Thus, the deviation from keplerian rotation, $(1-f^2)$, must grow in time: the disk becomes more magnetized and sub-keplerian with time because resistivity can only cause the redistribution of the magnetic field within the disk but cannot change the total flux.

Other properties of the disks can be calculated, e.g., the disk mass, the local dimensionless mass-to-flux ratio, and the Toomre Q parameter for axisymmetric stability. These are all functions of the radii and depend on the disk mass accretion rate, $\dot{M}_d$, the mass of the central star, M_*, the age of the system, $t_{\rm age}$, and the viscosity coefficient, D. Table 2 of S07 shows the application of these models to different young stellar objects. For the case of T Tauri stars, one requires a small value of $D = 10^{-2.5}$ or the disk size would be too large. In this table one can see that these models predict a substantial deviation from keplerian rotation for disks around T Tauri and FU Ori stars, with values of $f \sim 0.7$ and 0.4, respectively. For T Tauri stars, the uncertainties in the measured stellar masses are consistent with these values of f, and one requires independent mass estimates to determine if those disks are indeed sub-keplerian. In the case of the prototype FU Orionis, Donati et al. (2005) made spectropolarimetric observations and argued that there is sub-keplerian rotation in the disk at small radii because the observed high temperature lines are narrow. Also, the outer parts of the disks around low and high mass protostars are predicted to be unstable to gravitational fragmentation because the local mass-to-flux ratio is larger than 1 and the Q Toomre parameter is smaller than 1.

Table 1 shows the predicted magnitude of the magnetic field as functions of radius, ϖ, in disks around different young stars: T Tauri stars (TT), low mass protostars (LMP), FU Ori objects (FU Or), and high mass protostars (HMP). Paleomagnetic measurements from meteorites coming from the asteroid belt at 3 AU, indicate values of $B \sim 1$ G remnant of the magnetic fields in the primitive solar nebulae (e.g., Levy & Sonett 1978). In the case of FU Orionis, the observations of Donati et al. imply a magnetic field of 1 KG at 0.05 AU. Also, OH maser observations of around massive young stars give fields, $B \sim$ few mG, at distances of ~ 1000 AU, as shown, for example, in Figure 1 of Hutawarakorn & Cohen (2005). The location of the OH masers suggests that they are located in a disk, perpendicular to the outflow direction. Thus, the quoted values in Table 1 agree well with the observations.

TABLE 1

MODEL PREDICTIONS FOR DIFFERENT SYSTEMS

ϖ (AU)	TT/LMP	FU Or	HMP
0.05	302 G	1.92 KG	5.68 KG
3	1.09 G	6.85 G	20.5 G
100	8.74 mG	–	164 mG
1000	–	–	6.88 mG

The normalized vertical magnetic field in the disks, where the dependence on the stellar mass and disk accretion rate has been scaled out, is plotted in Figure 4 as a function of radius. We have assumed that the disk aspect ratio is a power-law with a slope, $(4\ell - 1)/2 = 1/4$. The measured magnetic fields for different objects are labeled in the figure and lie along the theoretical lines. Thus, our models are consistent with the measured magnetic fields over a large range of radii.

3.1. *Energy Dissipation in Magnetized Disks*

The process of resistive diffusion is a source of disk heating as is the viscous rubbing of adjacent disk rings. In our models, the rate of viscous dissipation per unit area (ergs s^{-1} cm^{-2}) is

$$\Psi = \nu\Sigma \left(\varpi \frac{d\Omega}{d\varpi}\right)^2 = \frac{3}{2} f^2 \left(\frac{GM_* \dot{M}_d}{2\pi\varpi^3}\right) . \qquad (19)$$

The rate of resistive dissipation per unit area is

$$Y \equiv \int_{-\infty}^{+\infty} \frac{\eta_{\rm local}}{4\pi} \left(\frac{\partial B_\varpi}{\partial z}\right)^2 dz = \eta \frac{(B_\varpi^+)^2}{8\pi z_0} . \qquad (20)$$

Thus, the ratio of both processes is given by

$$\frac{Y}{\Psi} = \frac{1}{3I_\ell} \left(\frac{1 - f^2}{f^2}\right) , \qquad (21)$$

and, for a given slope of the disk aspect ratio, ℓ, it depends only on the deviation from keplerian rotation, f. For large deviations from keplerian rotation, $f \sim 0.4$, both rates are equal, $Y \sim \Psi$. Nevertheless, for small deviations, $f > 0.9$, viscous dissipation dominates, $Y < 0.05\,\Psi$.

4. DISK WINDS

These models of magnetized accretion disks fulfill one criterion to eject disk winds

$$\frac{B_\varpi^+}{B_z} \geq \frac{1}{\sqrt{3}} ,$$

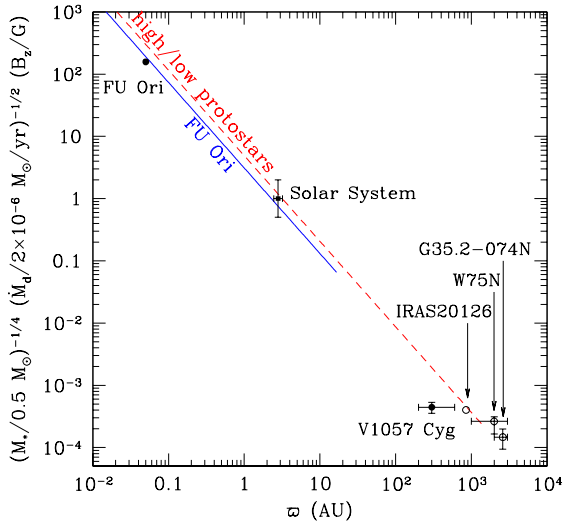

Fig. 4. Scaled magnetic field B_z vs. radius (Shu et al. (2007b).

i.e., the angle of the poloidal field with respect to the vertical is $\theta > 30°$ (Blandford & Payne 1982).

Nevertheless, to make the sonic transition (slow MHD), the square of the disk surface temperature must be

$$a_s^2 > \frac{1}{4}(1 - f^2)\frac{GM_*}{\varpi} , \qquad (22)$$

to climb the local potential well. Thus, sub-keplerian rotation in cold disks makes the sonic (slow MHD) point lie so many scale heights above the disk surface that the associated mass-loss rate would be too small (Shu et al. 2008). This problem is not alleviated by increasing the bending of the magnetic field lines. This is because how much **B** bends with respect to the vertical depends on the local fluid velocity and the rest of the field lines connected to infinity. Thus, the greater the bending, the greater the radial magnetic tension, and the greater deviation from keplerian rotation. Alternatively, disks surfaces can be heated by UV or FUV photons producing disk winds with important mass loss rates (e.g., Font et al. 2004; Lugo et al. 2005).

5. TIME DEPENDENT MODELS

We are currently working on time dependent models to follow the disk spreading. An example of a time dependent model is shown in Figure 5. This model has a mass-to-flux ratio $\lambda_0 = 4$ and a slope of the disk aspect ratio of 1/4. The upper left panel shows the deviation from keplerian rotation, f, as a function of the normalized disk radius, $\xi = \varpi/R_d(\tau)$, where $R_d(\tau)$ is the disk radius at a nondimensional

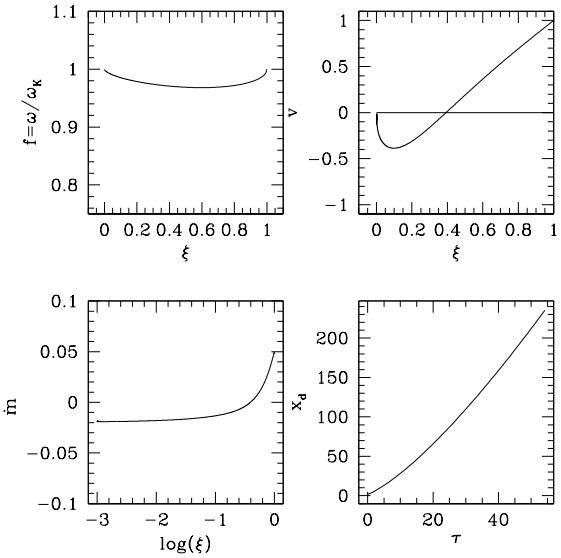

Fig. 5. Time dependent disk model.

time, $\tau = t/t_0$. The upper right panel shows the nondimensional velocity as a function of the normalized disk radius. The velocity is normalized using the outer edge disk velocity and is shown here only for illustration purposes. One can see that the inner disk is accreting and the outer disk is spreading out as angular momentum is redistributed by viscous torques. The lower panel shows the the nondimensional mass accretion rate, $\dot{m} = \sigma v x$, where σ is a nondimensional mass surface density, as a function of the normalized radius. One can see that the inner region achieves a constant value that corresponds to that of the steady-state models discussed above. Finally, the lower right panel shows that nondimensional disk radius, $x_d = R_d/R_0$, as a function of nondimensional time. For example, for a T Tauri system, with $M_* = 0.5\ M_\odot$, and a disk total angular momentum, $J_d = 50\ M_\odot$km s^{-1}, $R_0 = 23$ AU, and $t_0 = 1.8 \times 10^4$ yr.

6. CONCLUSIONS

We use mixing length arguments to derive expressions for the MRI viscosity, ν, and resistivity, η, in magnetized differentially rotating accretion disks. With these diffusivities, we find an analytic model of magnetized accretion disks in steady-state. The equations require a ratio of the resistivity to the viscosity coefficient, $\eta/\nu \propto z_0/\varpi \ll 1$, because the gas has to transport mass and angular momentum through field lines at compatible rates. This relation can be understood in terms of a loop dynamics, where mass is transported across field lines in magnetized loops that need to be twisted by differential rotation in order to reconnect with the downstream field line, and thus transport mass at an increase rate with respect to microscopic collisional values. Global MRI numerical simulations with dynamically strong **B** and non-zero flux are needed to compare with these results. The modeled disk structure (Σ, **B**) agree well with the observed properties of magnetized disks around young stars.

These models need a viscosity coefficient $D \sim 1$ except for the T Tauri disks, where $D \ll 1$. What physics determines the states with high or low viscosity? We speculate that MRI is well developed in high states, i.e., one has a large anomalous viscosity, ν, not constrained by collisional microscopic values. In a low state, the upper disk layers may be active (Gammie 1996) but loop twisting in 2D is not efficient, giving a small value for the coefficient $D \ll 1$. In this case, the resistivity η is quenched, given by collisional values. The relevant question is how can the disks go from a high state (FU Ori disks) to a low state (T Tauri disks)?

S. L. acknowledges support from PAPIIT-UNAM and CONACyT, México.

REFERENCES

Balbus, S. A., & Hawley, J. F. 1991, ApJ, 376, 214
Blandford, R. D., & Payne, D. G. 1982, MNRAS, 199,883
Donati, J.-F., Paletou, F., Bouvier, J., & Ferreira, J. 2005, Nature, 438, 466
Font, A. S., McCarthy, I. G., Johnstone, D., & Ballantyne, D. R. 2004, ApJ, 6007, 890
Galli, D., Lizano, S., Shu, F. H., & Allen, A. 2006, ApJ, 647, 374
Galli, D. Cai, M., Lizano, S., & Shu, F. H. 2009, RevMexAA (SC), 36, 143
Gammie, C. F. 1996, ApJ, 457, 355
Girart, J. M., Rao, R., & Marrone, D. P. 2006, Science, 313, 812
Gonçalves, J., Galli, D., & Girart, J. M. 2008, A&A, 490, L39
Hutawarakorn, B., & Cohen, R. J. 2005, MNRAS, 357, 338
Levy, E. H., & Sonett, C. P. 1978, in IAU Colloq. 52, Protostars and Planets, ed. T. Gehrels (Tucson: University of Arizona Press), 516
Lubow, S. H., Papaloizou, J. C. B., & Pringle, J. E. 1994, MNRAS, 268, 1010
Shu, F. H., Galli, D., Lizano, S., Glassgold, A. E., & Diamond, P. H. 2007a, ApJ, 665, 535 (S07)
Shu, F. H., Galli, D., Lizano, S., & Cai, M. J. 2007b, in IAU Symp. 243, Star-Disk Interaction in Young Stars, ed. J. Bouvier & I. Appenzeller (cambridge: Cambridge Univ. Press), 249
Shu, F. H., Lizano, S., Galli, D., Cai, M. J., & Mohanty, S. 2008, ApJ, 682, L121